

DESIGN AND OPTIMISATION OF A PLASMONIC REFRACTIVE INDEX SENSOR

By

Ahnaf Daiyan (180021303)
Dip Rahat Alam (180021306)
Md. Masum (180021316)

A Thesis Submitted to the Academic Faculty in Partial Fulfillment of the
Requirements for the Degree of

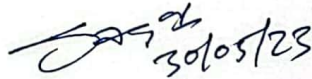
**BACHELOR OF SCIENCE
IN
ELECTRICAL AND ELECTRONIC ENGINEERING**



Department of Electrical and Electronic Engineering
Islamic University of Technology (IUT)
Board Bazar, Gazipur-1704, Bangladesh
May 2023

DESIGN AND OPTIMIZATION OF A PLASMONIC REFRACTIVE INDEX SENSOR

Approved by:



Handwritten signature and date: 30/05/23

Prof. Dr. Rakibul Hasan Sagor

Supervisor and Professor,
Department of Electrical and Electronic Engineering,
Islamic University of Technology (IUT),
Boardbazar, Gazipur-1704.

Declaration of Authorship

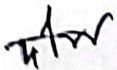
We, Ahnaf Daiyan (180021303), Dip Rahat Alam (180021306) and Md. Masum (180021316) hereby declare that the thesis titled "Design and Optimization of a Plasmonic Refractive Index Sensor" has been prepared by us and we confirm that:

- This thesis has been conducted as part of the requirements for the completion of our Bachelor of Science in Electrical and Electronic Engineering degree at the Islamic University of Technology (IUT).
- None of the content in this thesis has been submitted elsewhere for the purpose of obtaining any other Degree or Diploma.
- We have consistently provided clear attribution to the sources whenever we have referred to or consulted the published works of others.

Submitted By:



Ahnaf Daiyan (180021303)



Dip Rahat Alam (180021306)



Md. Masum (180021316)

Table of Contents

Declaration of Authorship.....	ii
Table of Contents	iii
List of Figures.....	v
List of Tables	vi
List of Acronyms	vii
Acknowledgements.....	viii
Abstract.....	ix
1 Introduction and Background	1
1.1 SURFACE PLASMON POLARITON	1
1.2 METAL-INSULATOR-METAL WAVEGUIDE TOPOLOGY	2
1.3 PLASMONIC REFRACTIVE INDEX SENSOR.....	3
1.4 LITERATURE REVIEW	4
1.5 THESIS OBJECTIVE	8
1.6 THESIS OUTLINE	8
2 Wave Theory and Material Modelling	10
2.1 ELECTROMAGNETIC WAVE THEORY	10
2.1.1 <i>Maxwell's Equation</i>	10
2.1.2 <i>Constitutive Relations</i>	11
2.1.3 <i>Wave Equation</i>	12
2.2 PLASMONIC MATERIAL MODELING	12
2.2.1 <i>The Drude model</i>	13
2.2.2 <i>The Lorentz Model</i>	15
2.2.3 <i>The Lorentz-Drude Model</i>	17
2.3 SIMULATION MODELING	17
2.3.1 <i>FEM for Electromagnetic Field Calculation</i>	17
2.3.2 <i>Scattering Boundary Condition (SBC)</i>	18

3	Performance Matrices of RI sensor and Re-simulation.....	19
3.1	RING RESONATOR.....	19
3.2	PARAMETERS OF SENSOR QUALITY	21
3.2.1	<i>Sensitivity (S)</i>	21
3.2.2	<i>Figure of Merit (FOM)</i>	22
3.2.3	<i>Quality Factor (Q-factor)</i>	23
3.3	RE-SIMULATION FOR QUALITY VALIDATION	23
4	Design, Optimization and Performance Analysis of the Proposed Device	
	27	
4.1	SENSOR DESIGN WITH DUAL OCTAGONAL STRUCTURE.....	27
4.1.1	<i>Basic Structure</i>	27
4.1.2	<i>Initial Transmission spectrum and results</i>	28
4.2	OPTIMIZATION FOR GAINING MAXIMUM SENSITIVITY	29
4.3	RESULT ANALYSIS	33
4.4	APPLICATION	33
5	Conclusion and Future work	34
5.1	CONCLUSION.....	34
5.2	FUTURE WORK	35
6	References.....	36

List of Figures

Figure 1.1: SPP propagation at the metal-dielectric interface [2].....	1
Figure 1.2: (a) and (b) Sensing mechanism illustration. (c) Shift of λ_{res} due to RI change [4].	3
Figure 1.3: plasmonic MIM waveguide-based RI sensors that have recently been developed by (a) Zhao et al. [20] (b) Al Mahmud et al. [21] (c) Xiao et al.[22] (d) Hayati & Khani [23] (e) Xie et al.[24] (f) Butt et al.[25].	6
Figure 2.1: Lorentz Model	16
Figure 3.1: Plasmonic waveguide coupled with ring resonator.....	19
Figure 3.2: Transmittance profile for the calculation of sensitivity	22
Figure 3.3: Transmittance profile for calculating FOM	22
Figure 3.4: Re-simulation of Al Mahmud et al. sensor [4].....	23
Figure 3.5: Representation of the simulation steps.....	24
Figure 3.6: Geometric structure and mesh view of Al Mahmud et al. [4].....	25
Figure 3.7: (a) Al Mahmud et al.'s [4] Transmission profile. (b) Re-simulated profile.	26
Figure 4.1: 2D Model of the proposed structure.....	27
Figure 4.2: Initial Transmission Spectrum	28
Figure 4.3: Optimization of radius (R) of resonators.....	29
Figure 4.4: Optimization of gap between resonators (g2).	30
Figure 4.5: Optimization of the width of the waveguide (w1).	31
Figure 4.6: Optimization of the width of the resonator (w2).....	31
Figure 4.7: Optimization of the gap between waveguide and resonator.	32
Figure 4.8: Transmission spectra of the optimized structure.....	33

List of Tables

Table 1.1: Comparison of performance metrics (sensitivity and FOM) of some different sensors.....	7
Table 3.1: Structural Parameters for Al Mahmud et al. [4]	24
Table 4.1: Initial Structural parameters of the proposed sensor	28
Table 4.2: Optimized structural parameters.....	32
Table 5.1: Overall performance metrics comparison of the proposed sensor with some recent <i>MIM</i> -based devices.	34

List of Acronyms

SPP	Surface Plasmon Polariton
SPR	Surface Plasmon Resonance
RI	Refractive Index
RIU	Refractive Index Unit
FEM	Finite Element Method
MIM	Metal Insulator Metal
IMI	Insulator Metal Insulator
FOM	Figure of Merit
FWHM	Full Width Half Maximum
TM	Transverse Magnetic

Acknowledgements

We would like to begin by expressing our gratitude to Allah (SWT), the most merciful and compassionate, for granting us the health, fortitude, and good fortune necessary to complete this task.

We would also like to express our gratitude to our thesis advisor, Dr. Rakibul Hasan Sagor, Professor, Department of Electrical and Electronic Engineering, Islamic University of Technology (IUT), for his consistent guidance and support throughout our studies and thesis work. With his zeal, eloquence, depth of knowledge, and perseverance, he always encouraged us to venture beyond our comfort zone.

We would also like to acknowledge all the faculty members of the Department of Electrical and Electronic Engineering at the Islamic University of Technology (IUT) for their encouragement and support.

Finally, we would like to express our deepest gratitude and appreciation to our parents, whose unwavering support and affection have been the foundation of this thesis. Their support, guidance, and sacrifices were crucial to our success, and we owe our accomplishments to their unwavering confidence in us.

Abstract

Plasmonics is a relatively new but emerging field. Extensive research is going on for the development of plasmonic devices because they have the capability to overcome some limitations of electronic devices. Our thesis focuses on the MIM waveguide configuration for a refractive index nano-sensor along with the incorporation of variously shaped resonators. By modifying the design specifications, the refractive index sensing property is explored thoroughly. The Finite Element Method (FEM) is employed to numerically analyze the transmission properties and sensitivity of the refractive index sensor in various configurations. The scattering boundary condition is implemented on the non-port boundary of the sensors. The detection of refractive index change has been numerically simulated and analyzed using COMSOL Multiphysics. The simulation environment has been validated by re-simulating an existing sensor from the literature. The sensitivity achieved using our proposed designs has been found to be 2586 nm/RIU, with a figure of merit (FOM) of 21.9 for the design with the ring-type dual octagonal resonator. It is shown that the sensor can detect refractive index changes for dielectrics whose refractive indices are between 1.30 and 1.40. The study demonstrates the maximum available sensitivity and figure of merit that will be suitable for using the device as a biosensor.

Chapter 1

Introduction and Background

Scientists are persistently striving to construct nano-scale devices that possess supplementary advantages, such as a sleek design, exceptional efficiency, and sophisticated aesthetics, in order to fulfill the demands of current technology. The utilization of metals holds significant importance in the advancement of these applications. Periodically, there is a constant emergence of novel findings concerning the performance of metals. These newly acquired knowledge plays a vital role in modifying the different structural parameters of metals to finely tune the interaction between light and metal to develop markedly improved photonic devices at subwavelength scales [1]. This synergistic interaction between light and metal is accurately explained by the theory of Surface Plasmon Polariton (SPP). In recent years, a substantial amount of research has been conducted on MIM waveguide-based surface plasmon polariton (SPP) sensors. Among these sensors, refractive index-based MIM sensors have emerged as particularly significant as they are highly sensitive to changes in the surrounding medium making them invaluable for biomaterial detection.

1.1 Surface Plasmon Polariton

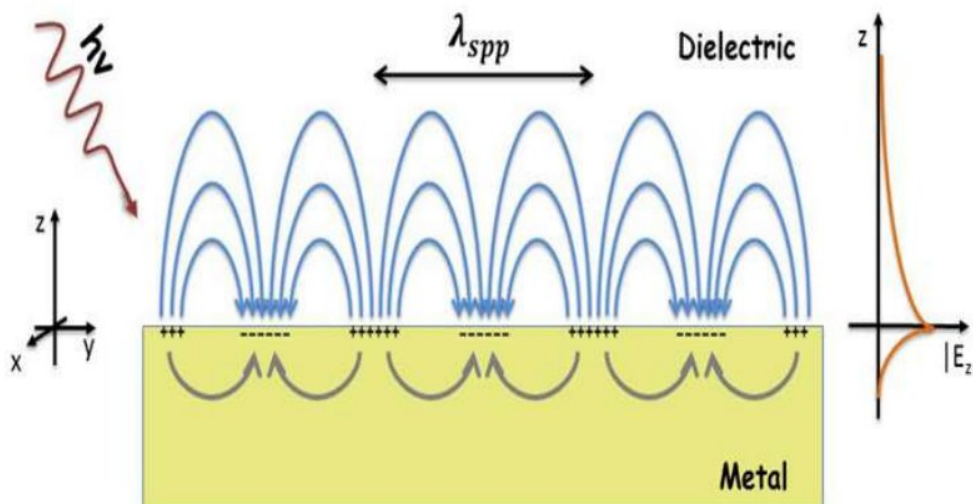


Figure 1.1: SPP propagation at the metal-dielectric interface [2]

Surface Plasmon Polariton (SPP) is a remarkable breakthrough in the field of metallic nanoplasmonics. It involves the interaction between incident photons and the oscillating surface electrons of a metal, leading to the propagation of an electromagnetic (EM) surface wave along the interface of the metal and dielectric at a resonant frequency. This intriguing interaction, occurring between the metal (with a relative permittivity, $\epsilon_r < 0$) and the dielectric (with a relative permittivity, $\epsilon_r > 0$), is commonly known as SPP [3]. As the distance from the interface increases within each medium, the magnitude of the surface wave experiences an exponential decay. In the dielectric medium, the wave's penetration depth, also known as the skin depth, is greater compared to the metal. According to specific literature, the skin depth for the metal is approximated to be around 10 nm, whereas for the dielectric, it typically exceeds 100 nm [4]. They possess remarkable capabilities in confining optical modes within sub-wavelength scales, making them highly valuable in various applications. This confinement results in an amplified electromagnetic field at the interface, endowing SPPs with a remarkable sensitivity to surface conditions. Consequently, these sensors possess unparalleled potential for detecting and analyzing surface properties and variations. SPPs possess a unique and distinctive capability to surpass the diffraction limit and confine light within subwavelength dimensions. This exceptional characteristic paves the way for the development of nanoscale plasmonic devices that have the potential to revolutionize various fields of research and applications [5]. SPPs serve as the fundamental building blocks of plasmonics, an emerging technology that finds applications in fully integrated optical instruments [6], sensors [7], filters [8], demultiplexers [9], and couplers [10].

1.2 **Metal-Insulator-Metal Waveguide Topology**

As previously stated in section 1.1, the production of surface plasmon polaritons (SPPs) at the interface requires the use of two materials characterized by positive and negative dielectric constants. Given that the dielectric constant of metals is negative, extensive research has been conducted to investigate different metallic nanostructures, aiming to harness the unique properties offered by SPPs [11]. Upon investigation of the SPP modes occurring at the interfaces of metal-dielectric layers, it is observed that these modes can be enhanced through two specific configurations: the insulator-metal-insulator (IMI) system, where a thin metal film is positioned between dielectrics, or the metal-insulator-metal (MIM) system, where a thin dielectric layer is encircled by metals [12]. The nanostructure utilizing the IMI configuration demonstrates a noteworthy capability for long-distance propagation. However, it exhibits

limited field localization along the interface [13]. Contrarily, the MIM waveguide, despite having significant propagation loss, has the ability to confine light within the subwavelength scale. This development creates an opportunity for integrating fully interconnected electronic circuits with optical circuits on a single chip, allowing for the utilization of both electrons and photons as information carriers. Thanks to its outstanding field confinement and exceptional sensitivity to the surrounding medium, the plasmonic refractive index (RI) sensor finds extensive usage in the detection of liquid temperature [14], concentration [15], and bio-material sensing applications [16].

1.3 Plasmonic Refractive Index Sensor

The refractive index sensor is considered a highly valuable component among plasmonic devices due to its ability to detect the refractive indices of diverse dielectric materials present within the sensor configuration. The MIM waveguide-based plasmonic refractive index sensors offer exceptional sensitivity to the structural parameters and surrounding media, thanks to the intense light-matter interaction near the metal-dielectric interface. These exceptional characteristic positions these sensors as highly promising candidates for nanoscale sensing applications, particularly when used to detect and track unknown substances, thus opening up new avenues in the field of nanoscale sensing.

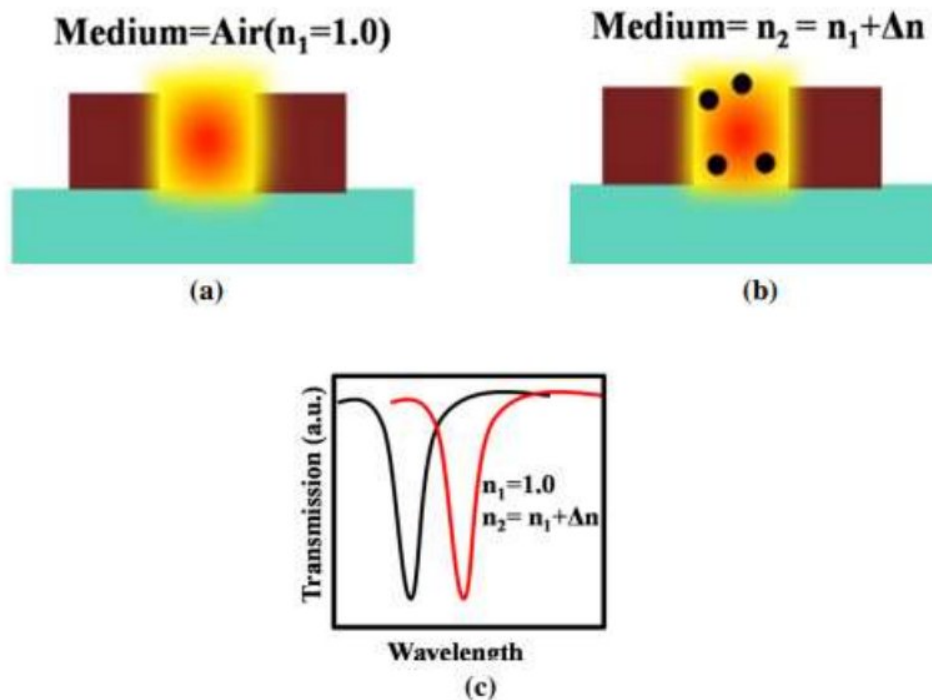


Figure 1.2: (a) and (b) Sensing mechanism illustration. (c) Shift of λ_{res} due to RI change [4].

Figure 1.2a illustrates the generation of SPPs at the interface when the sensing media is excited with a light source. A corresponding reduction in the transmittance curve is demonstrated in Figure 1.2c. Figure 1.2b depicts the variation in the effective refractive index (η_{eff}) of the MIM waveguide when a sample to be sensed is introduced. This alteration in η_{eff} induces a shift in the resonance wavelength (λ_{res}), as exhibited in Figure 1.2c. By measuring the displacement of λ_{res} , the plasmonic refractive index sensor can determine the refractive index of the unknown material being observed. The unidentified material within the MIM structure encompasses gaseous molecules, chemicals, bio-materials, and analogous substances. The implementation of SPPs within a MIM configuration provides advantageous opportunities for the development of compact integrated optical circuits. Furthermore, their effective utilization in on-chip applications has proven to be highly effective.

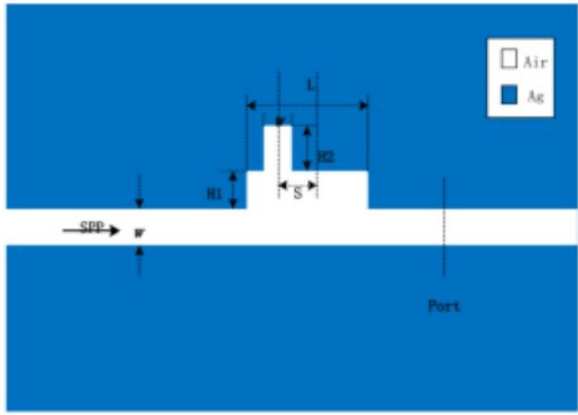
1.4 Literature Review

Significant research and development efforts have been dedicated to plasmonic sensors since the 1980s, reflecting the substantial efforts invested in advancing this field. Throughout the years, numerous plasmonic sensors have been developed, taking advantage of the remarkable properties of SPPs. Among these sensors, MIM based refractive index sensor has emerged as a prominent player in lab-on-chip bio-sensing applications. This sensor offers several advantageous features, including the capability to achieve deep subwavelength electromagnetic wave localization, ease of fabrication, label-free detection capabilities, and rapid response time [17]. Despite their advantages, nanoscale integrated MIM sensors often demonstrate lower sensitivity when compared to conventional bulky fiber optic sensors. To address this challenge, researchers have devoted their attention to enhancing the sensitivity of MIM sensors while maintaining other performance metrics. To achieve this, various approaches have been explored over the years, including coupling the MIM waveguide with ring cavities, nano-disc cavities, rectangular cavities, and other structural configurations [18-19]. These endeavors aim to enhance the sensitivity of MIM sensors without compromising their overall performance.

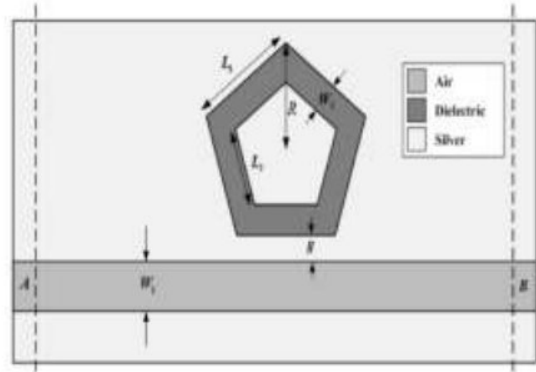
In 2018, Zhao et al. proposed a compact plasmonic structure composed of MIM waveguide coupled with groove and stub resonators (fig 1.3a) that provides a maximum sensitivity of 2000 nm/RIU [20]. In 2021, Al Mahmud et al. proposed a pentagonal structure (1.3b) having maximum sensitivity as high as 2325 nm/RIU [21]. A maximum sensitivity of 840 nm/RIU was recorded by Xiao et al. in 2021, when he proposed a tunable plasmonic sensor with Fano resonators in an inverted U-shaped resonator(1.3c)[22]. Also in 2021, Hayati & Khani

proposed an elliptical shaped resonator (1.3d) having the sensitivity value as high as 550 nm/RIU [23]. In 2023, Xie et al. demonstrated a structure consisting of a hexagonal resonator with a rotatable core and stub and tooth cavities coupled with a MIM waveguide, respectively [24]. Lately, Butt et al. proposed an RI sensor with a bow-tie configuration having a maximum sensitivity of 2300 nm/RIU [25].

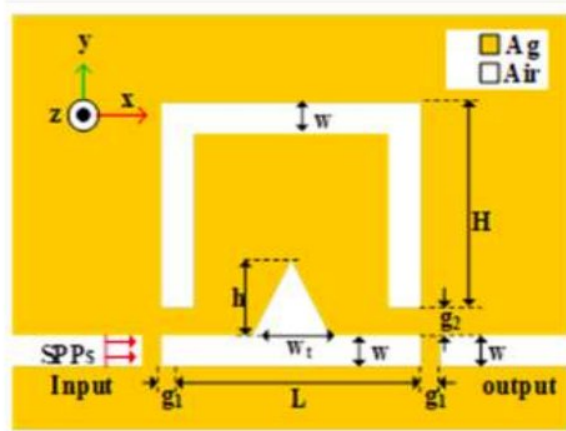
A comparison is provided for performance metrics, including sensitivity and FOM, among recently reported plasmonic sensors in table 1.1. The table presents details regarding the year of publication, structural design, and material model used in these sensors.



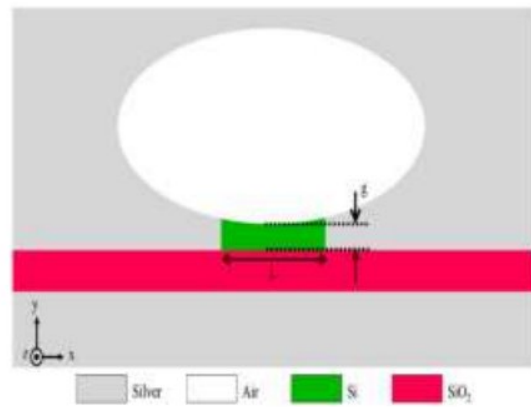
(a)



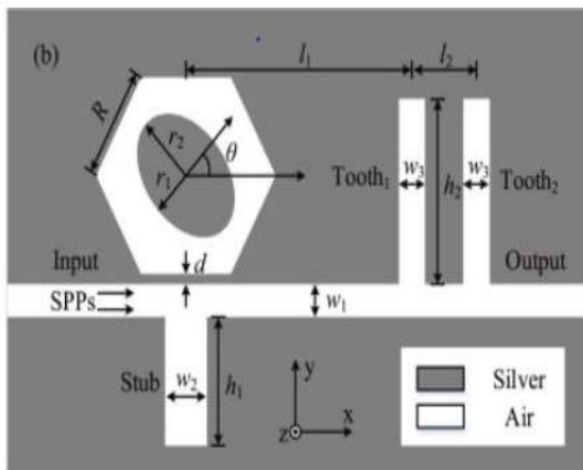
(b)



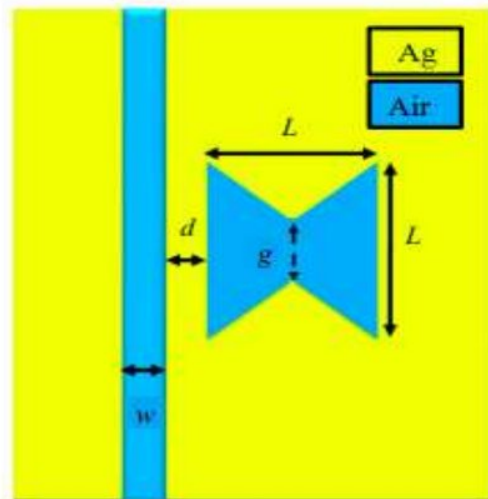
(c)



(d)



(e)



(f)

Figure 1.3: plasmonic MIM waveguide-based RI sensors that have recently been developed by (a) Zhao et al. [20] (b) Al Mahmud et al. [21] (c) Xiao et al. [22] (d) Hayati & Khani [23] (e) Xie et al. [24] (f) Butt et al. [25].

Table 1.1: Comparison of performance metrics (sensitivity and FOM) of some different sensors.

Ref.	Sensor Configuration	Metal Model	Sensitivity (nm/RIU)	FOM (RIU⁻¹)	Year
[26]	Stub and groove resonator	Drude	1260	-	2015
[27]	Fillet cavity	Drude	1496	124.6	2016
[28]	Nanorods in racetrack resonator	Lorentz-Drude	2610	52	2017
[29]	Multi-channel split ring resonator	Drude	1217	24.34	2018
[30]	Octagonal ring cavity	Lorentz-Drude	1540	-	2018
[31]	Two stub and one ring resonator	Debey-Drude	12622	280	2019
[33]	Square ring resonator	Lorentz-Drude	1200	19.7	2019
[32]	Square ring resonators with nanodots	Lorentz-Drude	907	40.8	2020
[25]	Bow-Tie Cavity	Lorentz-Drude	2300	31.5	2020
[34]	Three rectangular cavities	Drude	1516	14.83	2020
[23]	elliptical resonator	Drude	550	282.5	2021
[21]	Ring-Type Pentagonal Resonator	Lorentz-Drude	2325	46	2021
[22]	Inverted U-Shaped Resonator	Drude	840	3.9×10^5	2021

The main objective of including design variations, as outlined in table 1.1, is to enhance the device's ability to detect even the slightest disparity in the surrounding refractive index.

1.5 Thesis Objective

The objectives of this thesis are stated below:

- To design a highly sensitive RI sensor with MIM configuration
- To optimize the sensor structurally to increase the performance metrics of the sensor
- To investigate numerically the performance metrics of the newly optimized sensor
- To implement the design of the RI sensor in the form of a filter

1.6 Thesis Outline

Chapter 1 offers a brief introduction to surface plasmon polaritons and their significance in nanoscale communication. The chapter also explores recent advancements in refractive index sensors based on plasmonic MIM waveguides. Additionally, the chapter presents and discusses the outline of the thesis.

Chapter 2 primarily focuses on the fundamental wave equations, specifically Maxwell's equations, and discusses the modeling of metals. The chapter introduces three models: the Drude model, the Lorentz model, and the Lorentz-Drude model, which are employed to determine the permittivity of materials with respect to frequency. The discussion also encompasses the details of FEM and provides theoretical calculations for S-parameters and transmittance.

Chapter 3 is dedicated to the theoretical investigation of a ring resonator that employs a MIM configuration. The chapter extensively discusses the fundamental performance metrics employed for evaluating refractive index (RI) sensors. Additionally, the chapter includes the re-simulation of a previously published work using COMSOL Multiphysics software, which is then compared with the original study.

Chapter 4 is dedicated to the design of the proposed refractive index sensors. The chapter offers a detailed analysis of the initial structural design, the fabrication process, considerations for tolerance, and the performance evaluation of the sensors. The chapter extensively explores the performance parameters to gain a comprehensive understanding of the design parameters. Additionally, it showcases the applications of the proposed sensor designs as filters.

Chapter 5 serves as the culmination of the research, offering a thorough conclusion that evaluates and determines the best design in terms of sensitivity and FOM for the RI sensors examined in the literature. The chapter also explores potential plans and strategies for future improvements and enhancements.

Chapter 2

Wave Theory and Material Modelling

2.1 Electromagnetic Wave Theory

Due to the propagation of electromagnetic waves in the dielectric and electrons in the metal, *SPPs* are formed. The electromagnetic quality of waves is described by *Maxwell's* equations. These equations can be used to comprehend the propagation, interactions, and mutual influence of the electric and magnetic fields. EM waves propagate through a medium according to the wave equation, which can be derived from *Maxwell's* equations. The properties of the medium can be inferred from the medium's constituent parts. Silver and gold are the two most commonly used metals in plasmonic device design. Computational purposes necessitate material modelling and boundary conditions. One of the numerical techniques that can be used to calculate the electromagnetic field of a plasmonic device is the Finite Element Method (FEM). The transmittance of a device is the relationship between its input and output. With transmittance, the efficacy of plasmonic devices can be investigated.

2.1.1 Maxwell's Equation

Fundamental Laws

Maxwell's law, which is a compilation of four fundamental electromagnetic phenomena (*Faraday's law*, *Maxwell-Ampere's law*, and *Gauss' law* of the electric and magnetic forms), describes the relationship between electric and magnetic fields. Integral and differential forms of the equations are well-established and applied to the analysis of electromagnetic problems. Since the Finite Element Method (FEM) employs the differential form for numerical analysis, the differential form of *Maxwell's* equations is presented in this section. *Maxwell's* equation for time-varying electric and magnetic fields can be expressed as follows:

$$\text{Ampere – Maxwell Law} \quad : \nabla \times H = J + \frac{\partial D}{\partial t} \quad (2.1)$$

$$\text{Faraday's Law} \quad : \nabla \times E = -\frac{\partial B}{\partial t} \quad (2.2)$$

$$\text{Gauss' Law} \quad : \nabla \cdot D = \rho \quad (2.3)$$

$$\text{Gauss' Law for magnetism} : \nabla \cdot B = 0. \quad (2.4)$$

Here, E , H , D , B , J and ρ represent, respectively, electric field intensity, magnetic field intensity, electric flux densities, magnetic flux densities, electric current density, and volume charge density. The continuity equation, also known as the Law of Conservation of Charge, relates the electric current density to the volume charge density as follows:

$$\nabla \cdot J = -\frac{\partial \rho}{\partial t} \quad (2.5)$$

2.1.2 Constitutive Relations

Without specifying the generation of charge and current, the Maxwell equation explains the fields produced by charge and current. Constitutive equations describe the nature of the matter in contact with fields and permit the application of Maxwell's equation to a different substance. Constitutive equations are explained as follows:

$$D = \epsilon_0 E + p, \quad (2.6)$$

$$B = \mu_0 (H + M), \quad (2.7)$$

$$J = \sigma E. \quad (2.8)$$

Where,

ϵ_0 = Electric permittivity of vacuum, (Fm^{-1}),

μ_0 = Magnetic permeability of vacuum, (Hm^{-1}),

σ = Electric Conductivity, (Sm^{-1}).

The constitutive equation for linear materials with constant material properties regardless of the applied field is:

$$B = \mu_0 (1 + \chi_m) H = \mu_0 \mu_r H = \mu H, \quad (2.9)$$

$$D = \epsilon_0 (1 + \chi_e) E = \epsilon_0 \epsilon_r E = \epsilon E. \quad (2.10)$$

Here,

$$\epsilon_r = (1 + \chi_e),$$

$$\mu_r = (1 + \chi_m).$$

2.1.3 Wave Equation

Wave equation governs the propagation of electromagnetic waves. This can be deduced from equation 2.2 with ∇ , which yields:

$$\nabla \times (\nabla \times E) = \nabla \times \left(-\frac{\partial B}{\partial t} \right) = -\frac{\partial}{\partial t} (\nabla \times B). \quad (2.11)$$

From equation 2.1, 2.9 and 2.10 we get,

$$\nabla \times (\nabla \times E) = -\mu \varepsilon \frac{\partial^2 E}{\partial t^2}. \quad (2.12)$$

By taking, $\frac{\partial}{\partial t} = j\omega$, $\varepsilon = \varepsilon_0 \varepsilon_r$, and $\mu = \mu_0 \mu_r$ into consideration, the equation can be transformed as follows,

$$\nabla \times (\mu_r^{-1} \nabla \times E) - k^2 \varepsilon_r E = 0. \quad (2.13)$$

Where k_0 is the wave number and it can be expressed as,

$$k_0 = \omega \sqrt{\mu_0 \varepsilon_0} = \frac{\omega}{c_0}. \quad (2.14)$$

Equation 2.13 can be reformulated utilizing the relationship between refractive index n and ε_r , $\varepsilon_r = n^2$. Assuming $\mu_r = 1$, the following equation holds:

$$\nabla \times (\nabla \times E) - k^2 n^2 E = 0 \quad (2.15)$$

2.2 Plasmonic Material Modeling

At low frequencies or for extended wavelengths, metals are perfect conductors. As they have a negative field, they lack dispersive properties. However, at optical frequencies, metals exhibit a dispersive nature. At frequencies above the optical range, metals exhibit dielectric properties.

Three vectors can determine the behavior of a material in the presence of an externally oscillating electromagnetic field. They are E (intensity of the electric field), P (density of polarization), and D (electrical flux density).

They are presented as:

$$D(\omega) = \varepsilon(\omega)E(\omega) \quad (2.16)$$

$$P(\omega) = \varepsilon_0\chi(\omega)E(\omega), \quad (2.17)$$

$$D(\omega) = \varepsilon_0E(\omega) + P(\omega), \quad (2.18)$$

Combining equations 2.17 and 2.18 we get,

$$D(\omega) = \varepsilon_0E(\omega)(1 + \chi(\omega)). \quad (2.19)$$

The electrical susceptibility here is χ . The susceptibility is a dimensionless quantity that expresses how quickly a material becomes polarized in response to an applied electric field. Now that equations 2.16 and 2.19 have been compared, the relationship between permittivity and susceptibility is as follows:

$$\varepsilon(\omega) = \varepsilon_0(1 + \chi(\omega)), \quad (2.20)$$

Therefore, the relative permittivity is given by,

$$\varepsilon_r(\omega) = 1 + \chi(\omega). \quad (2.21)$$

In order to acquire the ideal response of a material to a specific electromagnetic excitation, the frequency-dependent permittivity and susceptibility of a dispersive material must be precisely modelled. Mathematically, the Drude model, Lorentz model, and Lorentz-Drude model are extensively employed to account for this dependence.

2.2.1 The Drude model

Paul Drude, the originator of the Drude model of an electric conductor, compares metal to a volume containing stationary positive ions surrounded by a gas of free-moving, non-interacting electrons. There are two forces operating on the electrons of metal, namely,

- Driving Force F_d
- Damping Force F_g

Driving and damping force are represented as,

$$F_d = qE = -eE, \quad (2.22)$$

$$F_g = -\Gamma v. \quad (2.23)$$

With opposite directions, the resultant of the two forces are,

$$F = F_d - F_g. \quad (2.24)$$

According to first law of motion by newton,

$$mr'' = -eE + \Gamma r'. \quad (2.25)$$

Here,

m = the mass of electron,

Γ = damping constant,

r = the displacement in meter,

v = electron's velocity, and

q = charge of electrons. Here, the prime represents differentiation order with respect to time.

The following equation describes the time harmonic electric field and time harmonic displacement:

$$E(t) = E_0 e^{-j\omega t} \Leftrightarrow E(\omega), \quad (2.26)$$

$$r(t) = R_0 e^{-j\omega t} \Leftrightarrow R(\omega). \quad (2.27)$$

The representation in frequency domain of equation 2.25 is,

$$mR''(\omega) - \Gamma mR'(\omega) + eE(\omega) = 0, \quad (2.28)$$

The frequency domain derivatives will yield,

$$-m\omega^2 R''(\omega) + j\omega\Gamma mR'(\omega) + eE(\omega) = 0. \quad (2.29)$$

Simplifying the expression 2.25,

$$R(\omega) = \frac{-e}{m(j\Gamma\omega - \omega^2)} E(\omega), \quad (2.30)$$

The polarization for n number of electrons is calculated as follows:

$$P(\omega) = -neR(\omega), \quad (2.31)$$

Or,

$$P(\omega) = \frac{e^2 n}{m(j\Gamma\omega - \omega^2)} E(\omega), \quad (2.32)$$

The susceptibility derived from the preceding equation is denoted as,

$$\frac{P(\omega)}{\varepsilon_0 E(\omega)} = \frac{e^2 n}{\varepsilon_0 m(j\Gamma\omega - \omega^2)} = \chi(\omega), \quad (2.33)$$

Substituting this value into equation 2.10,

$$\varepsilon_r(\omega) = 1 + \frac{e^2 n}{\varepsilon_0 m(j\Gamma\omega - \omega^2)}, \quad (2.34)$$

If we assume ω_p to be the plasma frequency, we will obtain:

$$\omega_p^2 = \frac{e^2 n}{\varepsilon_0 m}. \quad (2.35)$$

Taking into account the frequency-dependent flux density to be,

$$D(\omega) = \varepsilon_0 \left(1 + \frac{\omega_p^2}{j\Gamma\omega - \omega^2} \right) E(\omega), \quad (2.36)$$

At low frequency, 1, which diminishes the dispersive relationship with,

$$D(\omega) = \varepsilon_0 \left(1 - \frac{\omega_p^2}{\omega^2} \right) E(\omega). \quad (2.37)$$

2.2.2 The Lorentz Model

Figure 2.1 demonstrates that the Lorentz model depicts the atom in a much simpler manner. This model is very useful for visualizing the interaction between atoms and fields. This model explains the relationship between the smaller mass electron and the larger mass nucleus, where electrons are bound to atoms and cannot move freely. Thus, a restoring force, F_r , which is expressed as F_r , acts between them.

$$F_r = -kr. \quad (2.38)$$

Here, spring constant is represented by k and the unit is Newtons per meter.

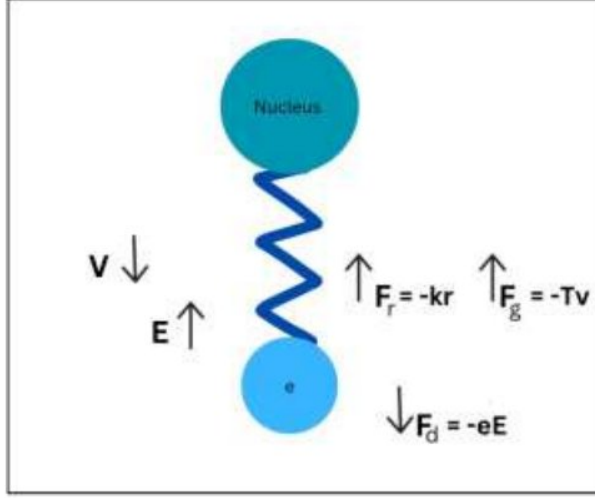


Figure 2.1: Lorentz Model

By the Law of Motion,

$$mr'' + \Gamma mr'(\omega) + mkr + eE = 0 \quad (2.39)$$

The frequency domain representation of Equation 2.39 is shown as,

$$R(\omega)(m\omega_0^2 + j\omega\Gamma m - m\omega^2 - eE(\omega)) = 0 \quad (2.40)$$

By taking natural frequency, $\omega_0 = \sqrt{\frac{k}{m}}$,

$$R(\omega) = \frac{-e}{m(\omega_1^2 + j\omega\Gamma - \omega^2)} E(\omega). \quad (2.41)$$

Therefore, the susceptibility can be expressed as:

$$\frac{P(\omega)}{\varepsilon_0 E(\omega)} = \frac{e^2 n}{\varepsilon_0 m(\omega_0^2 + j\omega\Gamma - \omega^2)} = \chi(\omega). \quad (2.42)$$

Therefore, from equation 2.19, the frequency domain expression for D is,

$$D(\omega) = \varepsilon_0 \left(1 + \frac{\omega_p^2}{\omega_0^2 + j\omega\Gamma - \omega^2} \right) E(\omega) \quad (2.43)$$

2.2.3 The Lorentz-Drude Model

The Lorentz-Drude model is the most general description of the electromagnetic field incident on metal. This model specifies two distinct categories of electrons oscillating within the metal, which contribute to the permittivity of the metal as a whole. The Drude model is best suited for electrons that are free, while the Lorentz model is best suited for electrons that are bound. Therefore, the permittivity of the Lorentz-Drude model is,

$$\varepsilon = \varepsilon_{free} + \varepsilon_{bound}, \quad (2.44)$$

Where,

$$\varepsilon_{free} = 1 + \frac{\omega_p}{j\Gamma\omega - \omega^2},$$
$$\varepsilon_{bound} = \frac{\omega_p}{\omega_0 + j\omega\Gamma - \omega^2}.$$

Combining the model and frequency domain representation of the electric field's characteristic D is,

$$D(\omega) = x_0 \left(1 + \frac{\omega_p}{j\Gamma\omega - \omega^2} + \frac{\omega_p^2}{\omega_0 + j\omega\Gamma - \omega^2} \right). \quad (2.45)$$

The Lorentz-Drude model is denoted by the expression 2.45.

2.3 Simulation Modeling

2.3.1 FEM for Electromagnetic Field Calculation

The finite element method (*FEM*) solves problems of complex geometry and inhomogeneous media more effectively than other mathematical methods that are conceptually simpler and easier to code, such as the finite difference method, method of moments (*MOM*), etc.

Using *Maxwell's* equation, electromagnetic fields are computed. The expressions for the electrical voltage V , and the magnetic potential vector A are:

$$B = \nabla \times A, \quad (2.46)$$

$$E = -\nabla \times V. \quad (2.47)$$

Considering equation 2.46, it is possible to transfer equation 2.2 into,

$$\nabla \times E = -\nabla \times \left(\frac{\partial A}{\partial t} \right) \quad (2.48)$$

As the electric field potential for the non-static fields is increased with an induced volt-age,

$$E = -\nabla V - \left(\frac{\partial A}{\partial t}\right). \quad (2.49)$$

Conductors replace the term charge density with a boundary equation of the Dirichlet type.

The potential equation can be rewritten as a Laplace equation,

$$\nabla \cdot (\varepsilon \nabla V) = 0 \quad (2.50)$$

Here, represents a diagonal tensor, while the off-diagonal coupling terms are ignored:

$$\varepsilon = \begin{bmatrix} \varepsilon_x & 0 & 0 \\ 0 & \varepsilon_y & 0 \\ 0 & 0 & \varepsilon_z \end{bmatrix} \quad (2.51)$$

The energy of the electric field is expressed as:

$$W_E = \int_V \frac{D \cdot E}{2} dV = \int_V \frac{\varepsilon |E|^2}{2} dV \quad (2.52)$$

Scattering parameters can be evaluated using the equation,

$$S_{ij} = \frac{\int_{\text{porti}} (E_j \cdot E_i^*) dA_i}{\int_{\text{porti}} (E_j \cdot E_j^*) dA_i} \quad (2.53)$$

T represents the time average reflection and transmittance coefficient. T can be obtained by,

$$T = |S_{ij}|^2 \quad (2.54)$$

2.3.2 Scattering Boundary Condition (SBC)

By employing scattering boundary condition (*SBC*) at the simulation window, a transparent boundary condition for incoming and outgoing (scattered) incident waves is achieved.

Outgoing (scattered) wave is defined as:

$$E = E_{SC} e^{-jk(n \cdot r)} + E_0 E^{-jk(K \cdot r)}, \quad (2.55)$$

Where E_0 is the incident plane wave propagating in the direction of k . The boundary condition is completely transparent for perpendicular scattered plane waves and partially transparent for oblique incident scattered plane waves.

Chapter 3

Performance Matrices of RI sensor and Re-simulation

3.1 Ring Resonator

The primary structure of a ring resonator is depicted in Fig.3.1. It has a straight wave guide along with a ring shaped resonator of radius R. The relation between the input excitation and output can be expressed as [35]

$$\begin{bmatrix} E_{t1} \\ E_{t2} \end{bmatrix} = \begin{bmatrix} t & k \\ -k^* & t^* \end{bmatrix} \begin{bmatrix} E_{i1} \\ E_{i2} \end{bmatrix} \quad (3.1)$$

Here, E_{i1} is the amplitude of complex mode of the source at the input port and E_{t1} is the amplitude of complex mode of transmission at the output port. E_{i2} is referred as the amplitude of complex mode of coupled component to the resonator cavity and E_{i2} is the amplitude of complex mode of transmitted component from the resonator cavity. k and t are the parameters that depends on coupling mechanism. A ‘*’ as superscript on these terms represents the complex conjugate of the respective terms.

The reciprocal nature of the networks makes the matrix symmetric. Hence,

$$|k^2| + |t^2| = 1 \quad (3.2)$$

Considering E_{i1} equals unity for simplification,

$$E_{i2} = \alpha \cdot e^{j\theta} E_{t2} \quad (3.3)$$

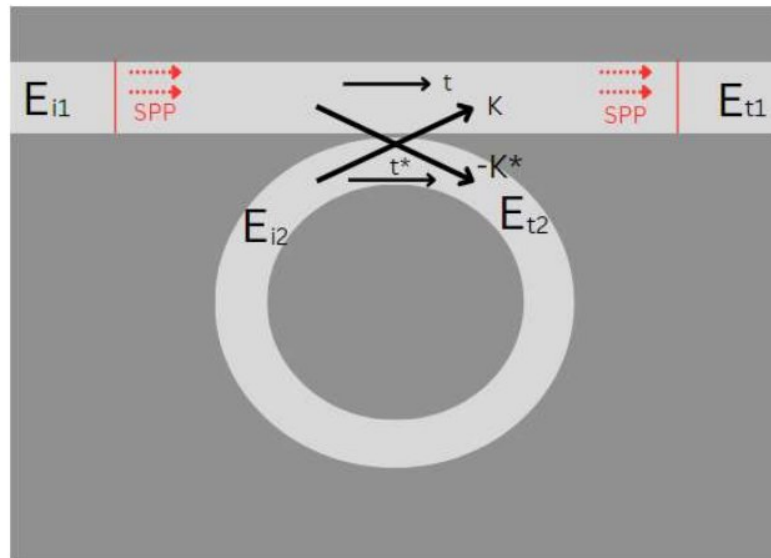


Figure 3.1: Plasmonic waveguide coupled with ring resonator.

Where, α is the coefficient loss of the ring and θ is presented as,

$$\theta = \frac{\omega L}{c} = \frac{2\pi c_0 L}{\lambda_c} = k \cdot \eta_{eff} \cdot L = \beta \cdot L \quad (3.4)$$

The phase velocity of the ring resonator is represented by c , which is given by, $c = \frac{c_0}{\eta_{eff}}$.

Where, η_{eff} indicates the effective refractive index and L represents effective propagation length of the coupled wave.

From Equation (3.1) and (3.3) we get,

$$\begin{aligned} E_{t2} &= -k^* + t^*(\alpha e^{j\theta} E_{t2}), \\ E_{t2}(1 - t^*\alpha e^{j\theta}) &= -k^*, \\ E_{t2} &= \frac{-k^*}{1 - t^*\alpha e^{j\theta}} \end{aligned} \quad (3.5)$$

$$E_{t1} = \frac{-\alpha + t e^{-j\theta}}{-\alpha t^* + e^{-j\theta}} \quad (3.6)$$

$$E_{i2} = \frac{-\alpha k^*}{-\alpha t^* + e^{-j\theta}} \quad (3.7)$$

While on resonance $\theta + \varphi_t = 2\pi m$ and the coupling loss is given by $t = |t|e^{j\varphi_t}$. Here φ_t denotes the coupling phase and m is an integer. The transmission power of the waveguide is given by P_{t1} while the circulating power inside the ring cavity is P_{i2} .

$$P_{t1} = |E_{t1}|^2 = \frac{\alpha^2 + |t|^2 - 2\alpha|t| \cos(\theta + \varphi_t)}{1 + \alpha^2|t|^2 - 2\alpha|t| \cos(\theta + \varphi_t)} = \frac{(\alpha - |t|)^2}{(1 - \alpha|t|)^2} \quad (3.8)$$

$$P_{i2} = |E_{i2}|^2 = \frac{\alpha^2(\alpha - |t|)^2}{(1 - \alpha|t|)^2} \quad (3.9)$$

At resonance condition, the expression for resonant wavelength λ_m can be derived as,

$$\frac{2\pi}{\lambda_m} \cdot \eta_{eff} \cdot L = 2\pi(m - \frac{\varphi_t}{2\pi}) \quad (3.10)$$

$$\lambda_m = \frac{\eta_{eff} \cdot L}{m - (\frac{\varphi_t}{2\pi})} \quad (3.11)$$

For initiating input excitation, light is injected into the waveguide. Halogen lamp technology is useful in this purpose. It has a wide light spectrum containing the entire wavelength range where λ_m is expected to exist. For establishing fundamental TM_0 mode propagation of electromagnetic wave, $w \ll \lambda_{incident}$. The dispersion equation of this mode can be expressed as [36],

$$\begin{aligned}
\tanh\left(\frac{k_{MUS} * w}{2}\right) &= -\frac{\epsilon_{MUS} * k_{Silver}}{\epsilon_{Silver} * k_{MUS}}, \\
k_{MUS,silver} &= \sqrt{\beta_{SPP}^2 - \epsilon_{MUS,silver} * k_0^2}, \\
\eta_{SPP} &= \frac{\beta_{SPP}}{k_0} = \frac{2\pi}{\lambda}
\end{aligned} \tag{3.12}$$

Where, the width of wave guide is represented as w . The dielectric constant of MUS and Silver are given by ϵ_{MUS} and ϵ_{Silver} respectively. The effective refractive index η_{SPP} is expressed as the ratio between propagation constant, β_{SPP} and free space wave number, k_0 .

3.2 Parameters of Sensor Quality

The performance of the sensor needs to be evaluated to understand the effectiveness of the sensor. To do so, there are some parameters which are measured. For a Plasmonic refractive index sensor, its sensitivity depends on the structural parameters such size of waveguide, size of resonator cavity, etc. By evaluating the sensors performance, its parameters are tuned to obtain an optimized sensor of higher efficiency. Some determinants of performance of Plasmonic RI sensors are Sensitivity (S), figure of merit (FOM), quality factor (Q -factor), etc.

3.2.1 Sensitivity (S)

Different types of structures, such as double cavities and ring resonators, are intended to produce spectral responses with Lorentzian peaks and Fano resonances. In order for the sensor to detect the refractive index, the material whose index is to be measured must be inserted in the cavity. The wavelength of the resonance exhibits red shift or blue shift if there is a change in the refractive index. The definition of sensitivity is the alteration of resonance wavelength ($\Delta\lambda$) in response to a unit change of the refractive index (n). The mathematical expression is given as [37],

$$S = \frac{\Delta\lambda}{\Delta n} \tag{3.13}$$

Where, Δn is the change in refractive index whereas $\Delta\lambda$ is the change in wavelength as depicted in figure 3.2. The measurement of the transmittance dip shift can be achieved through the

utilization of a contemporary spectrometer. As a result, the sensitivity of a refractive index sensor can be readily computed.

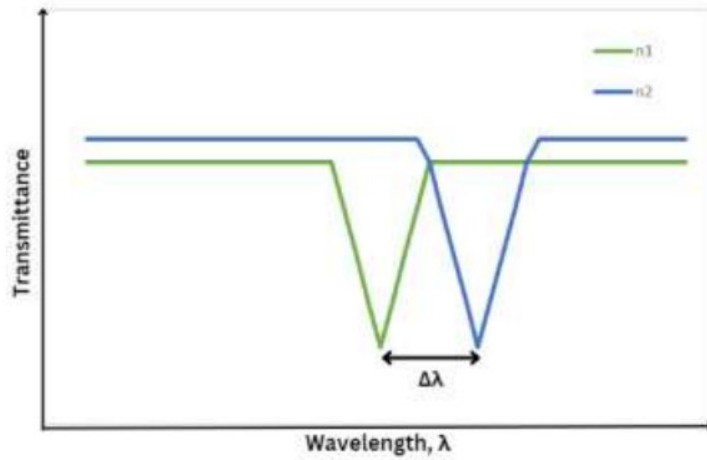


Figure 3.2: Transmittance profile for the calculation of sensitivity

3.2.2 Figure of Merit (*FOM*)

FOM stands for Figure of Merit. It is commonly employed in sensing applications to assess sensing efficacy. It is mathematically represented as,

$$FOM = \frac{S}{FWHM} \quad (3.14)$$

Where, *S* represents Sensitivity and FWHM represents Full Width Half Maximum. FWHM

$$FWHM = \lambda_2 - \lambda_1 \quad (3.15)$$

is obtained by,

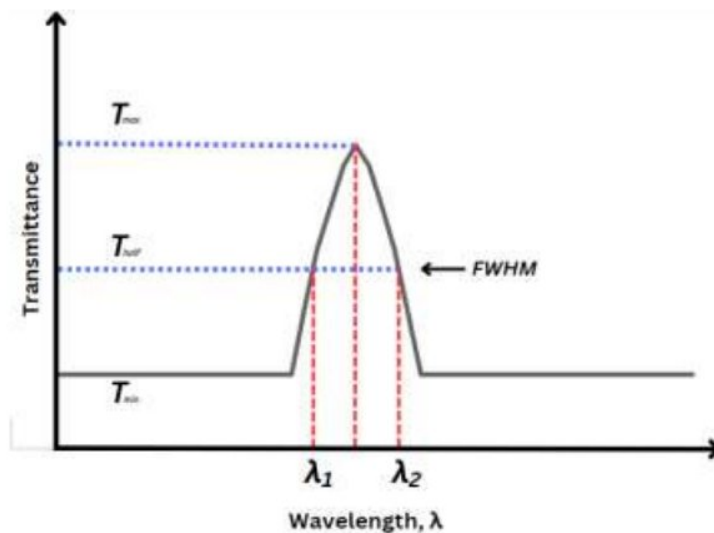


Figure 3.3: Transmittance profile for calculating FOM

Here, λ_2 and λ_1 are wavelength values at T_{half} . We can obtain T_{half} from figure 3.3,

$$T_{half} = \frac{T_{max} - T_{min}}{2}$$

3.2.3 Quality Factor (*Q-factor*)

Sensors possessing a high Q-factor exhibit suitability for a broad spectrum of applications, such as narrow-bandwidth filters, high-efficiency nonlinear optical devices, high-performance lasers, and high-sensitivity sensors. The mathematical expression for the Q-factor can be stated as follows:

$$Q - factor = \frac{\lambda_{res}}{FWHM} \quad (3.16)$$

Here, λ_{res} is the resonance wavelength

3.3 Re-simulation for Quality validation

The simulation setup must be validated before designing our own models. So the re-simulation of some already published papers are verified in this section. “Plasmonic Refractive Index Sensor Based on Ring-Type Pentagonal Resonator with High Sensitivity” proposed by Al Mahmud et al., [38] is re-simulated in this section. Figure 3.4 exhibits the structure of the proposed sensor and table-3.1 contains the geometric parameters of the structure.

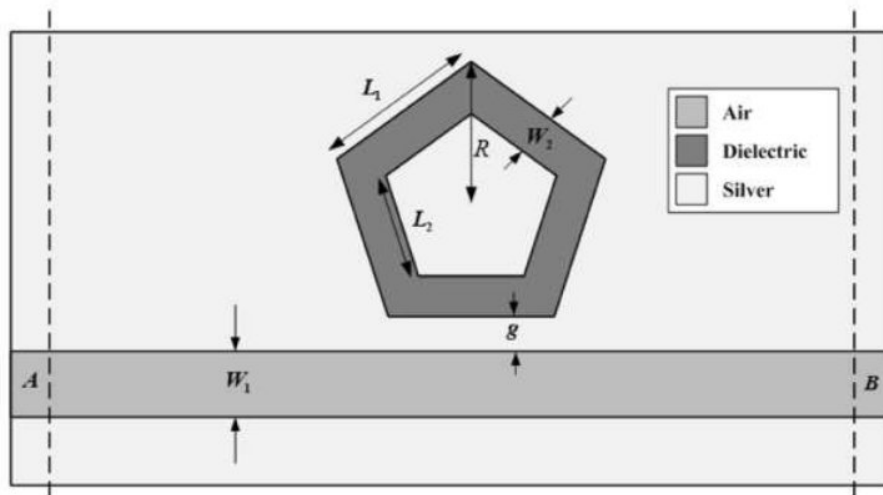


Figure 3.4: Re-simulation of Al Mahmud et al. sensor [38]

Design Parameters	Value (nm)		Denoted Symbol
	For max Sensitivity	For max FOM	
Gap between waveguide and ring resonator	32	32	g
Width of ring resonator	70	70	W_2
Radius of inscribed pentagonal ring	331	235	R

Table 3.1: Structural Parameters for Al Mahmud et al. [38]

The parameters of the structure of the sensor is kept same and its transmission profile is re-evaluated using COMSOL Multiphysics Software. Initially a two dimensional Finite Element Method (FEM) scheme is selected. The physics is selected as EMFD (Electromagnetic wave frequency domain). Then the structural parameters, defining the geometry of the sensors are

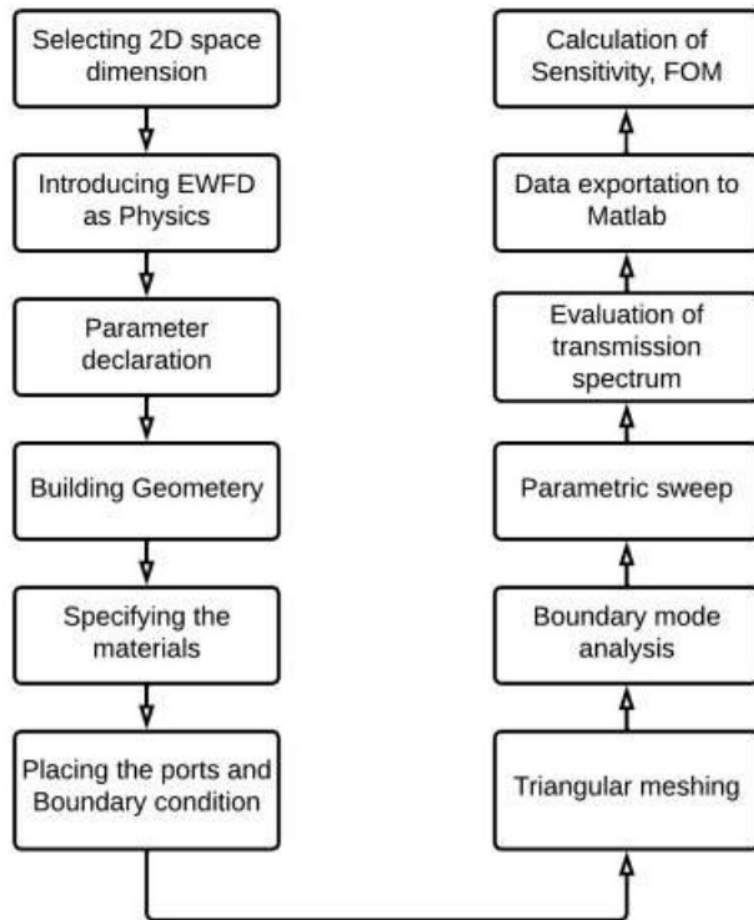


Figure 3.5: Representation of the simulation steps

declared. The desired geometric shape is then constructed. Different parts of the sensor constitutes different materials. Different materials are allocated in their respective places. Subsequently ports and boundary conditions are assigned. For discretizing the structure and obtaining better accuracy, extra fine meshing is applied. Figure 3.6 shows the geometry construction and the meshed structure respectively using COMSOL Multiphysics software.

Parametric sweep is utilized to observe the effect of variation of different parameters on the

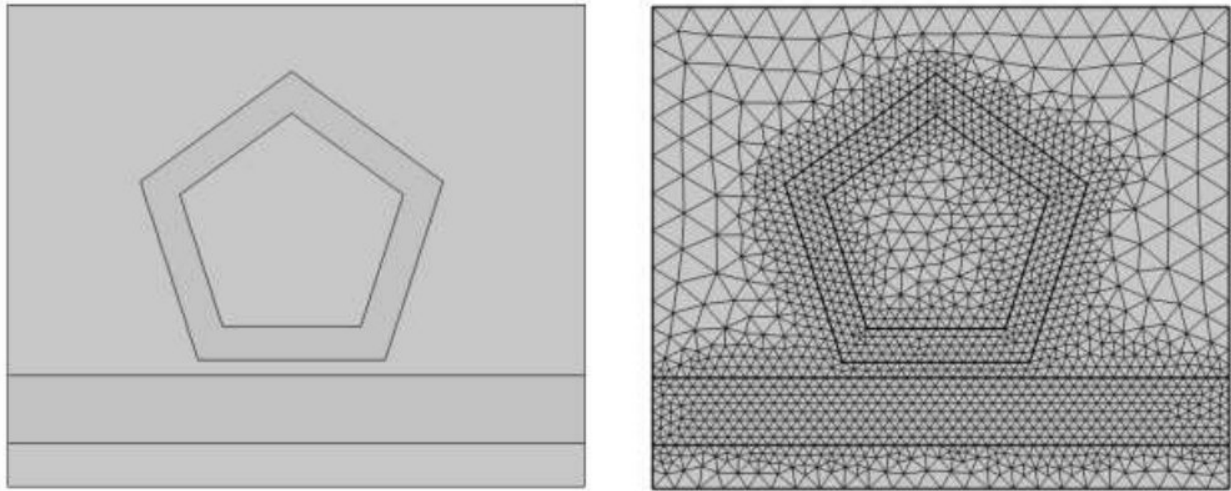
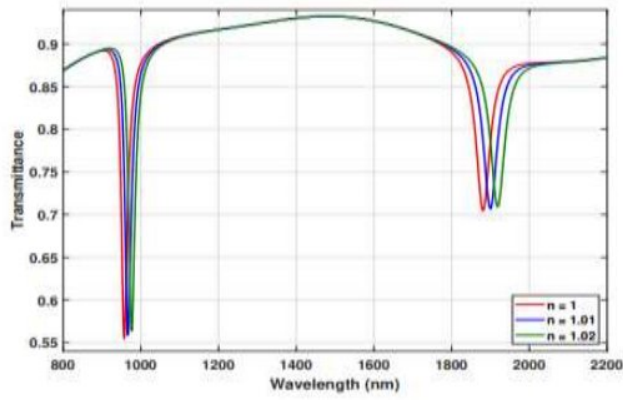
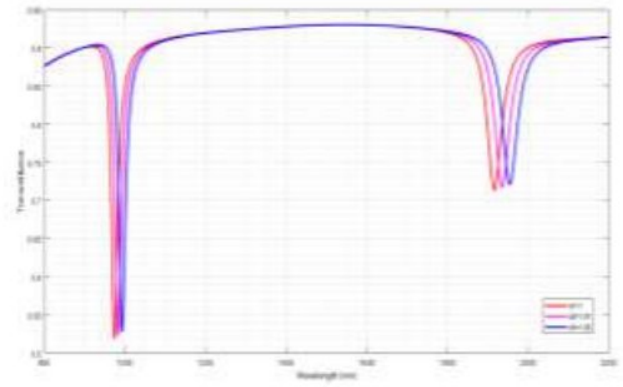


Figure 3.6: Geometric structure and mesh view of Al Mahmud et al. [38]

simulation. The obtained transmission spectra is then analyzed to evaluate the sensors performance and tune the parameters accordingly. Finally the sensitivity is calculated after exporting the simulated data. The transmission spectrum of the original work and re-simulated work is depicted in figure 3.6 (a, b) respectively. The spectrum was analyzed for a refractive index variation of $n = 1, 1.01$ and 1.02 . After using sensitivity equation, the calculated result was found to be 2343 nm/RIU . The published result is 2325 nm/RIU . There is a very slight difference between the published result and simulated result and it is within the allowable range. So we can say that our simulation setup is appropriate for carrying out the performance analysis of the sensor



(a)



(b)

Figure 3.7: (a) Al Mahmud et al.'s [38] Transmission profile. (b) Re-simulated profile.

Chapter 4

Design, Optimization and Performance Analysis of the Proposed Device

4.1 Sensor Design with dual octagonal structure

4.1.1 Basic Structure

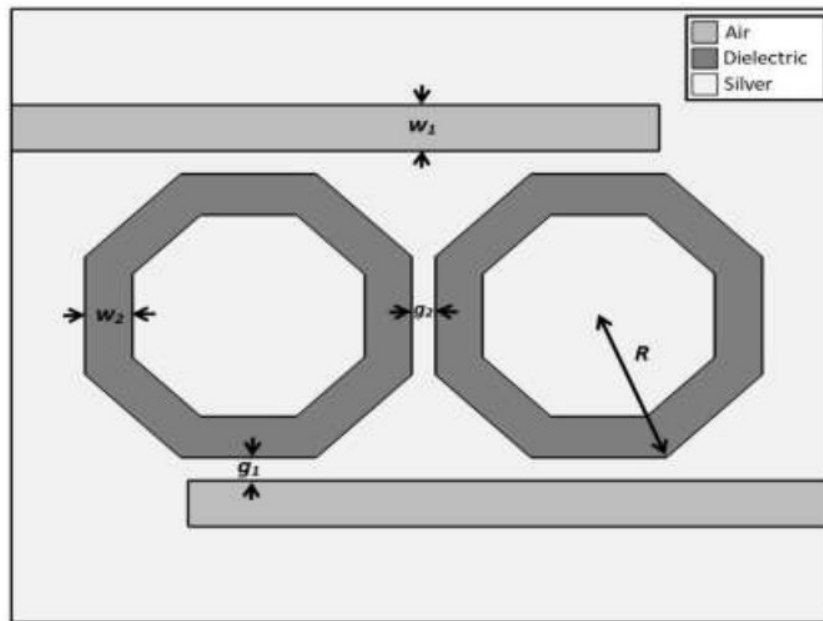


Figure 4.1: 2D Model of the proposed structure

The 2D configuration of the proposed sensor is given in figure 4.1. It consists of MIM waveguide along with dual octagonal ring resonators. The initial structural parameters for modeling the sensor in 2D is listed in table 4.1. The dark grey color in figure 4.1 represents the dielectric material or the material under sensing (MUS) which are filled into the cavities of the ring resonator. The white color in the figure denotes silver which is used as a metallic base. FEM mode is used to solve the differential equations for numerically analyzing the transmittance spectrum of the sensor. COMSOL Multiphysics software is utilized for this purpose.

Specifications	Value (nm)
Core radius of the octagonal resonator (R)	230
Gap between the waveguide and octagonal resonator (g_1)	12
Gap between the octagonal resonators (g_2)	25
Width of the waveguide (w_1)	45
Width of the octagonal Resonator (w_2)	30

Table 4.1: Initial Structural parameters of the proposed sensor

While performing the simulation, two ports are selected. The transmission of SSP through the output port is measured with respect to the input port. This measures the transmittance. Mathematically it is calculated as $T = \frac{P_{output}}{P_{input}}$.

4.1.2 Initial Transmission spectrum and results

COMSOL Multiphysics software is utilized to simulate the structure with MUS having refractive index range of 1.32 to 1.40 with a step difference of 0.02. Figure 4.2 depicts the transmission spectrum with the initial geometric configuration.

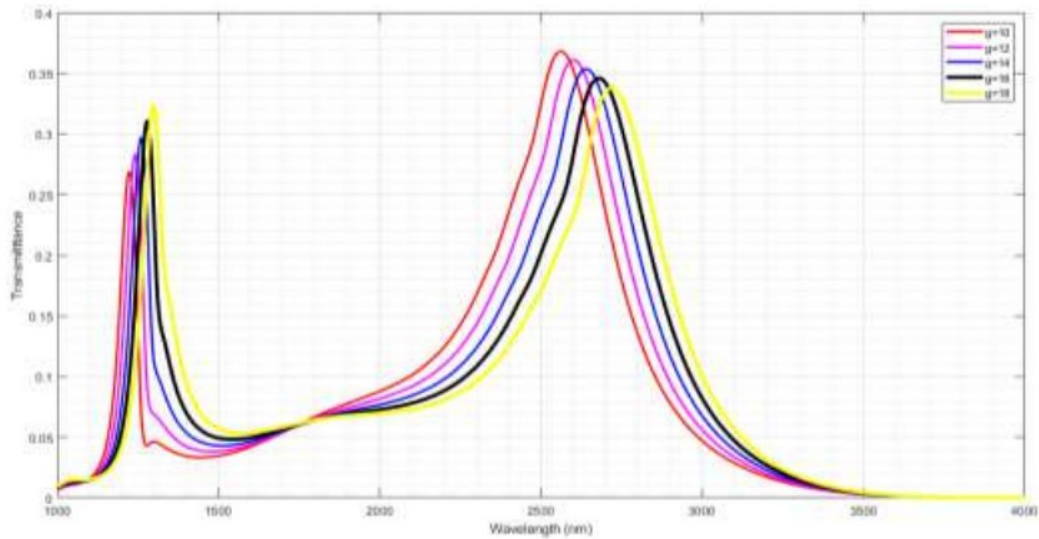


Figure 4.2: Initial Transmission Spectrum

The transmission spectrum has two modes. The maximum sensitivity for mode 1 is 1020.6 nm/RIU and for mode 2, it is 2218.3 nm/RIU.

4.2 Optimization for gaining maximum sensitivity

For obtaining optimal performance, the parameters mentioned in table 4.1 needs to be optimized.

After performing simulations multiple times, it has been observed that five parameters out of all, greatly influences the performance of the structure. These are radius of the inscribed octagonal resonator (R), gap between resonators (g2), width of waveguide (w1), width of resonator (w2) and gap between waveguide and resonator (g1).

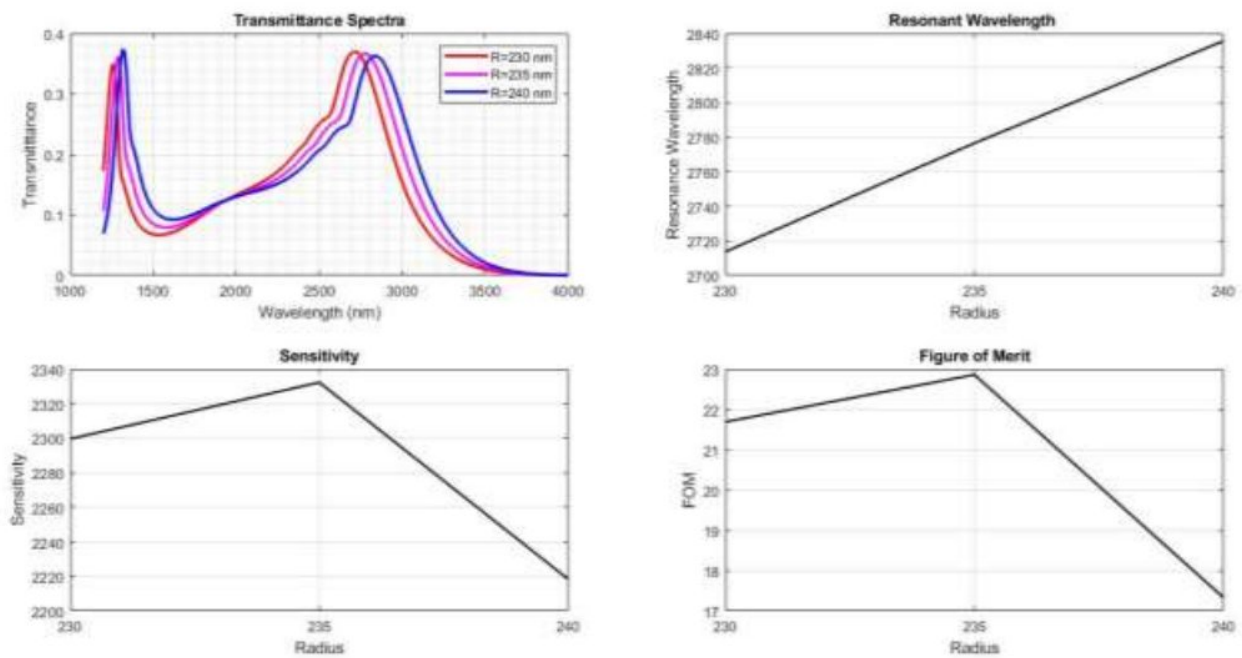


Figure 4.3: Optimization of radius (R) of resonators.

First of all, the radius (R) of the inscribed octagonal resonator is optimized. In figure 4.3, the transmittance spectra along with the resonant wavelength, sensitivity and FOM are visualized. Here we can observe that a maximum sensitivity of 2332.3 nm/RIU and a FOM of 22.86 can be achieved when the value of R is 235 nm. Hence, to optimize the sensor for optimal performance, the value of R is chosen as 235 nm.

Secondly, the gap between resonators (g_2) is optimized. For this purpose, simulation is performed by varying the value of g_2 from 20 nm to 30 nm with a step of 5 nm. From figure 4.4, we can observe that a maximum sensitivity of 2458.2 and a FOM of 19.2 can be achieved when g_2 is 20 nm.

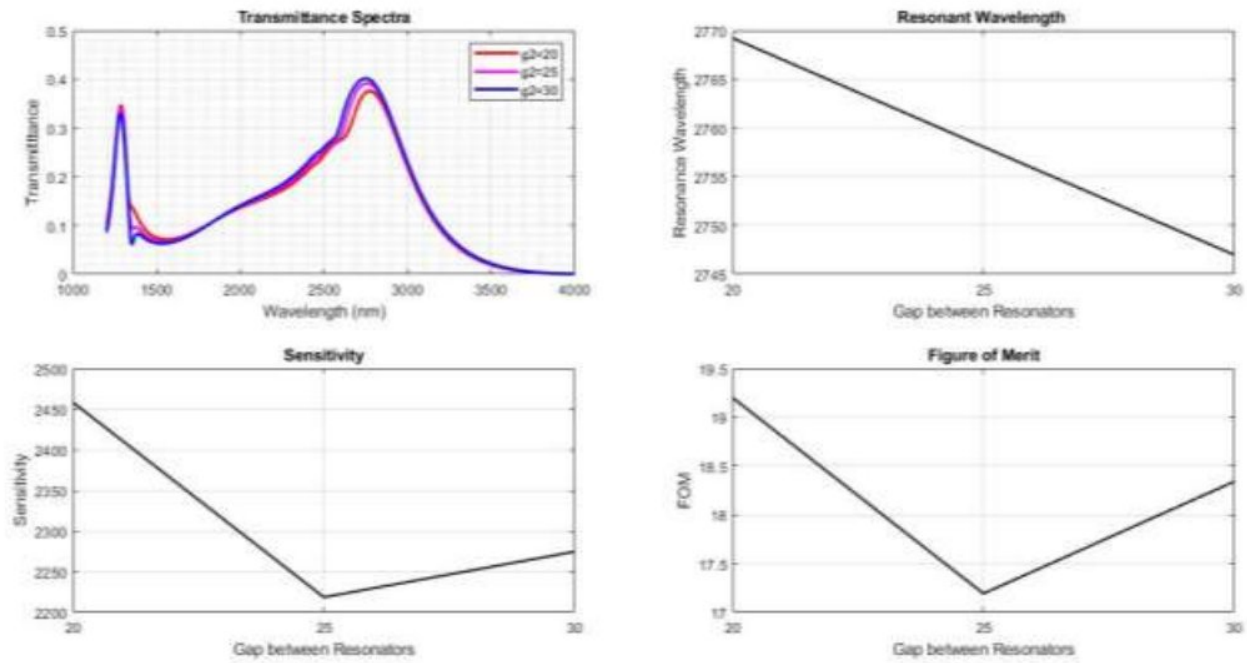


Figure 4.4: Optimization of gap between resonators (g_2).

Thirdly, the width of the waveguide is optimized. In the proposed sensor design, there is MIM (Metal Insulator Metal) wave guide in which a dielectric material is sandwiched between two metal claddings. The width of the waveguide is varied to observe the transmission spectra. For this purpose, a parametric sweep is performed. The results of the simulation, along with the values of sensitivity and FOM, are depicted in figure 4.4. It can be observed that for an optimized value of 40 nm width, a maximum sensitivity of 2586.2 nm/RIU and 21.51 FOM is achieved.

Fourthly, the width of the ring resonator is tuned for optimal sensor performance. Simulations are performed for different values of w_2 , and transmission spectra are shown in figure 4.5. The sensitivity and FOM of the sensor for different widths of the resonator cavity are also depicted in the figure. From this, it can be observed that when w_2 is 40 nm, the maximum sensitivity of

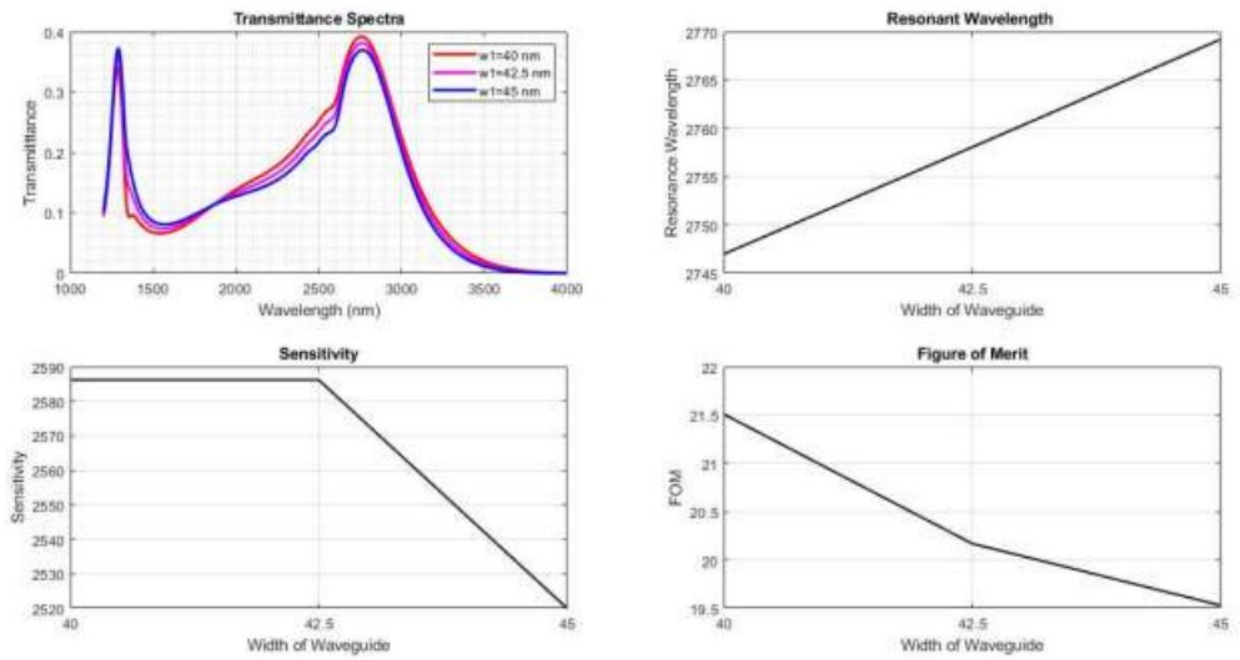


Figure 4.5: Optimization of the width of the waveguide (w_1).

2586.2 is attained. The FOM at this condition is 20.04, which is smaller than when the width is 50nm. However, as a very low sensitivity is obtained for that value of w_2 , a compromise in FOM has to be made to maximize sensitivity.

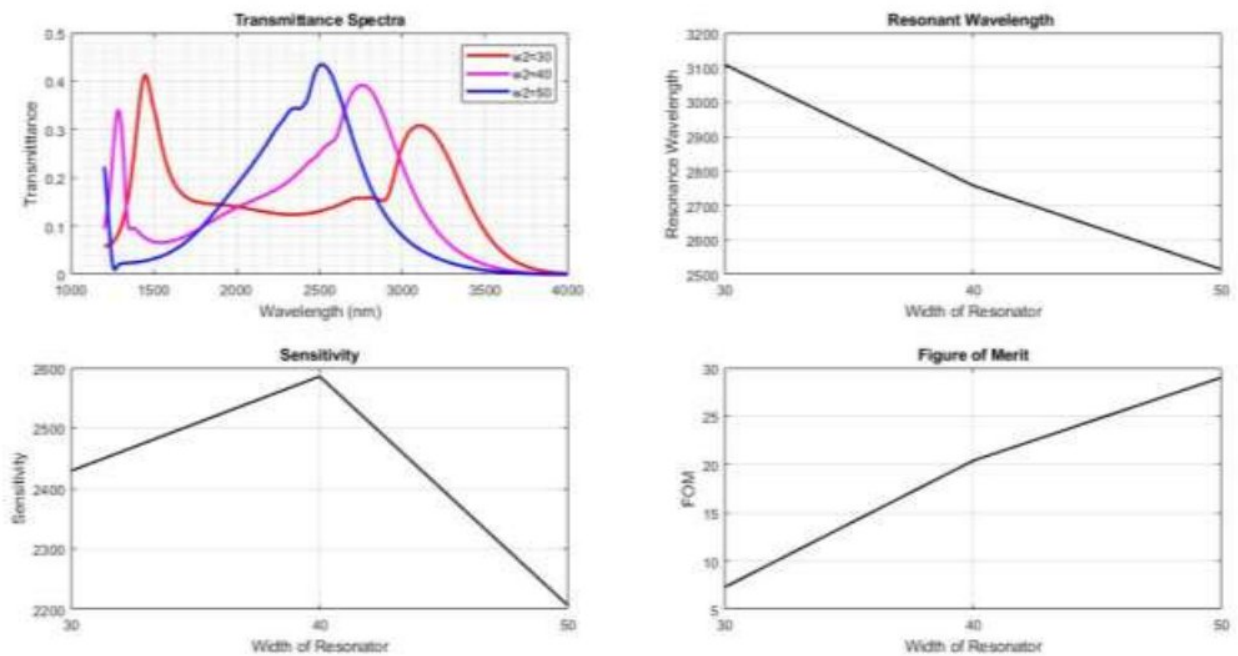


Figure 4.6: Optimization of the width of the resonator (w_2)

Finally, the gap between waveguide and resonator (g_2) is taken as a structural parameter that needs to be analyzed to enhance the performance of the device. To do so, simulations are performed to obtain the values of sensitivity and FOM for different values of g_2 . The results of the simulations are represented in Figure 4.6. It can be observed that when g_2 is 10nm, the highest sensitivity of 2586.2 is obtained with a FOM of 19.74. As this value of g_2 gives maximum sensitivity, it is considered the length of gap between waveguide and resonator in the optimized final structure.

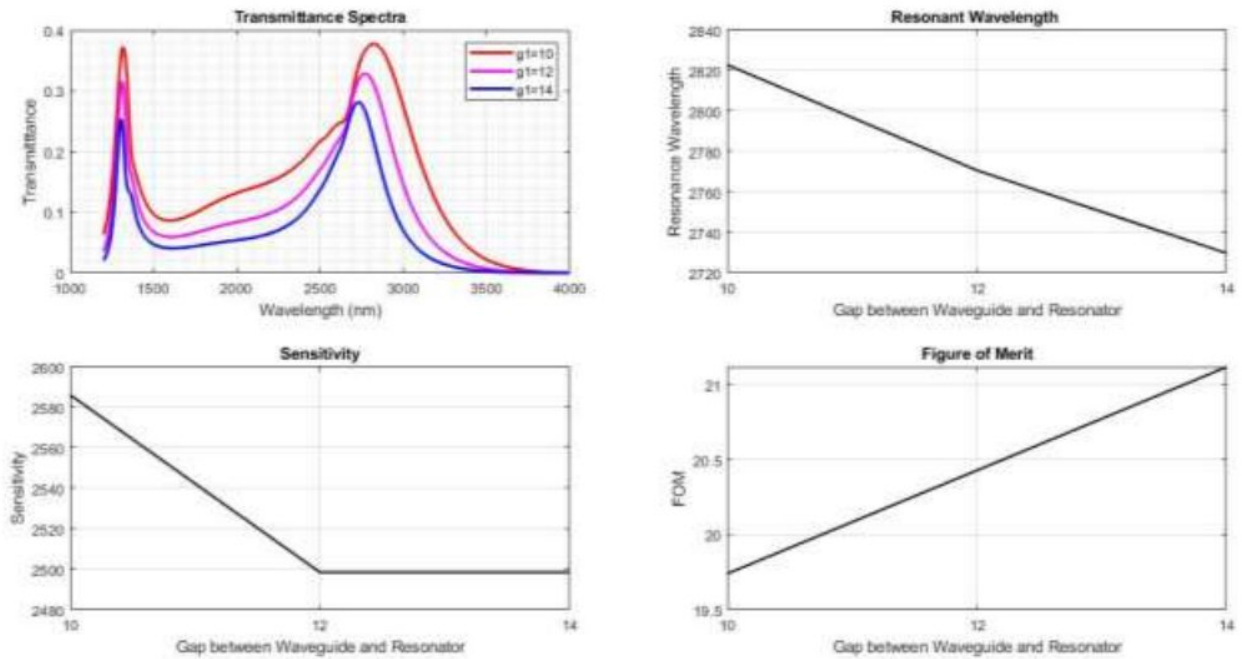


Figure 4.7: Optimization of the gap between waveguide and resonator.

After analyzing the simulation results, the final optimized parameters are depicted in Table 4.2.

Specifications	Value (nm)
Core radius of the octagonal resonator (R)	235
Gap between the waveguide and octagonal resonator (g_1)	10
Gap between the octagonal resonators (g_2)	20
Width of the waveguide (w_1)	40
Width of the octagonal Resonator (w_2)	40

Table 4.2: Optimized structural parameters.

4.3 Result Analysis

The geometry was constructed utilizing the optimized parameters and the transmission spectrum was simulated as Figure 4.6.

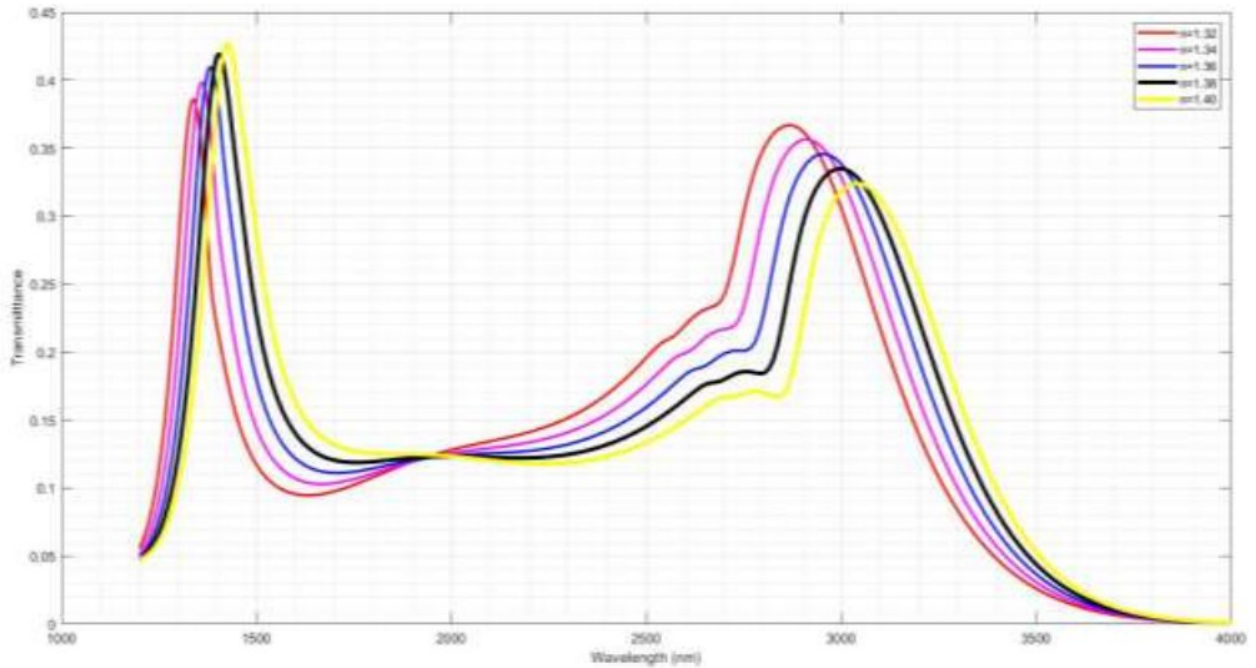


Figure 4.8: Transmission spectra of the optimized structure

This transmission spectra has two modes. For mode 1, we can obtain a maximum sensitivity of 1140 nm/RIU with 21.9 FOM. For mode 2, a maximum sensitivity of 2586 nm/RIU can be achieved with a FOM value of 11.4.

4.4 Application

The proposed sensor can be used as a biosensor to detect biological components for which the refractive indices are known. Cancerous cells such as Jurkat, HeLa, PC12, MBA-MD-231, MCF-7, and Basal have refractive indices ranging from 1.36–1.4. For example, normal basal cells have a refractive index of 1.36, whereas cancerous cells have a refractive index of 1.38 [39]. These fall within the range of the sensor’s sensitivity, as the proposed sensor can detect refractive indices from 1.30 to 1.40 and shows a maximum sensitivity of 2586 nm/RIU. So the sensor can work as a biosensor that can detect these cancerous cells.

Chapter 5

Conclusion and Future work

5.1 Conclusion

This thesis presents a refractive index (RI) sensor utilizing a MIM configuration, incorporating two octagonal ring resonators. To investigate the performance of the proposed devices, the FEM scheme in the COMSOL Multiphysics Software is utilized to analyze their transmission and propagation spectra. Sensitivity refers to the change in resonant wavelength corresponding to a unit change in refractive index. FOM is a metric used to assess the performance of a sensor based on its sensitivity and narrow linewidth. It provides an indication of the sensor's efficiency and effectiveness.

In order to enhance the sensing capability and FOM, a step-by-step optimization process is followed for the structural parameters of the sensor. At optimized parameter values of $R=235$ nm, $g_1=10$ nm, $g_2=20$ nm, $w_1=40$ nm and $w_2=40$ nm, the proposed structure exhibits an overall maximum sensitivity and FOM of 2586 nm/RIU and 21.9 respectively. Table 7.1 presents a comparison of the performance metrics between the proposed sensor and several similar works. The sensor's higher sensitivity, compact size, and label-free detection capabilities make it well-suited for a variety of applications in the field of bio-sensing.

Table 5.1: Overall performance metrics comparison of the proposed sensor with some recent *MIM*-based devices.

Ref.	Year	Sensitivity (nmRIU ⁻¹)	FOM
Chen et al. [26]	2015	1260	-
Chen et al. [27]	2016	1496	124.6
Tang et al. [34]	2017	1125	75
Ghorbani et al. [30]	2018	1540	-
Butt et al. [33]	2019	1200	19.7
Zhang et al. [34]	2020	1516	14.83
Xiao et al. [22]	2021	840	3.9×10^5
Proposed Structure	2023	2586	21.9

5.2 Future Work

This thesis focuses on optimizing a two octagonal ring resonator-based RI sensor with a MIM configuration, where silver is used as the metal. In the future, the following measures can be taken into consideration to further enhance the performance of the MIM-based plasmonic sensor.

- To mitigate the propagation loss and enhance the overall performance of the sensor, alternative materials with varying doping concentrations can be employed.
- The structure can be optimized to attain both maximum sensitivity and a higher FOM.
- By investigating different material options, alternatives that can potentially improve the sensors' overall performance can be found in the future.
- Incorporating machine learning techniques can significantly enhance the optimization process in the future.

References

- [1] W. L. Barnes, A. Dereux, and T. W. Ebbesen, "Surface plasmon subwavelength optics," *nature*, vol. 424, no. 6950, pp. 824–830, 2003.
- V. V. Temnov, G. Armelles, U. Woggon, D. Guzatov, A. Cebollada, A. GarciaMartin, J.-M. Garcia-Martin, T. Thomay, A. Leitenstorfer, and R. Bratschitsch, "Active magneto-plasmonics in hybrid metal–ferromagnet structures," *Nature Photonics*, vol. 4, no. 2, pp. 107–111, 2010.
- [2] Z. Han and S. I. Bozhevolnyi, *Waveguiding with surface plasmon polaritons*. Elsevier B.V., 2014, vol. 4. [Online]. Available: <http://dx.doi.org/10.1016/B978-0-444-59526-3.00005-7>
- [3] D. K. Gramotnev and S. I. Bozhevolnyi, "Plasmonics beyond the diffraction limit," *Nature photonics*, vol. 4, no. 2, pp. 83–91, 2010.
- [4] N. Kazanskiy, S. Khonina, and M. Butt, "Plasmonic sensors based on metalinsulator-metal waveguides for refractive index sensing applications: A brief review," *Physica E: Low-dimensional Systems and Nanostructures*, vol. 117, p. 113798, 2020.
- [5] W. L. Barnes, A. Dereux, and T. W. Ebbesen, "Surface plasmon subwavelength optics," *Nature*, vol. 424, no. 6950, pp. 824–830, aug 2003. [Online]. Available: <http://www.nature.com/articles/nature01937>.
- [6] S. A. Maier and H. A. Atwater, "Plasmonics: Localization and guiding of electromagnetic energy in metal/dielectric structures," *Journal of Applied Physics*, vol. 98, no. 1, 2005.
- [7] M. F. Hassan, R. H. Sagor, I. Tathfif, K. S. Rashid, and M. Radoan, "An optimized dielectric-metal-dielectric refractive index nanosensor," *IEEE Sensors Journal*, vol. 21, no. 2, pp. 1461–1469, 2020.
- [8] Y.-J. Guo, K.-D. Xu, X. Deng, X. Cheng, and Q. Chen, "Millimeter-wave onchip bandpass filter based on spoof surface plasmon polaritons," *IEEE Electron Device Letters*, vol. 41, no. 8, pp. 1165–1168, 2020.
- [9] E. Forati and G. W. Hanson, "Surface plasmon polaritons on soft-boundary graphene nanoribbons and their application in switching/demultiplexing," *Applied Physics Letters*, vol. 103, no. 13, p. 133104, 2013.

- [10] R. H. Sagor, M. S. I. Sumon, and M. Tazwar, "Design and analysis of a novel air gap-based semi-elliptical nanoplasmonic coupler," *Plasmonics*, vol. 14, no. 6, pp. 1993–2001, 2019.
- [11] J. J. Burke, G. I. Stegeman, and T. Tamir, "Surface-polariton-like waves guided by thin, lossy metal films," *Physical Review B*, vol. 33, no. 8, pp. 5186–5201, 1986.
- E. N. Economou, "Surface plasmons in thin films," *Physical Review*, vol. 182, no. 2, pp. 539–554, 1969.
- [12] R. Zia, M. D. Selker, P. B. Catrysse, and M. L. Brongersma, "Geometries and materials for subwavelength surface plasmon modes," *Journal of the Optical Society of America A*, vol. 21, no. 12, p. 2442, 2004.
- [13] M. F. Hassan, R. H. Sagor, I. Tathfif, K. S. Rashid, and M. Radoan, "An optimized dielectric-metal-dielectric refractive index nanosensor," *IEEE Sensors Journal*, vol. 21, no. 2, pp. 1461–1469, 2020.
- [14] Y.-F. C. Chau, "Mid-infrared sensing properties of a plasmonic metal–insulator–metal waveguide with a single stub including defects," *Journal of Physics D: Applied Physics*, vol. 53, no. 11, p. 115401, 2020.
- [15] S. Ghorbani, M. Sadeghi, and Z. Adelpour, "A highly sensitive and compact plasmonic ring nano-biosensor for monitoring glucose concentration," *Laser Physics*, vol. 30, no. 2, p. 026204, 2019.
- [16] Z. Zhang, J. Yang, X. He, J. Zhang, J. Huang, D. Chen, and Y. Han, "Plasmonic refractive index sensor with high figure of merit based on concentric-rings resonator," *Sensors*, vol. 18, no. 1, p. 116, 2018
- [17] M. Butt, N. Kazanskiy, and S. Khonina, "Nanodots decorated asymmetric metal–insulator–metal waveguide resonator structure based on fano resonances for refractive index sensing application," *Laser Physics*, vol. 30, no. 7, p. 076204, 2020.
- [18] M. R. Rakhshani and M. A. Mansouri-birjandi, "Sensors and Actuators B: Chemical High sensitivity plasmonic refractive index sensing and its application for human blood group identification," *Sensors & Actuators: B. Chemical*, vol. 249, pp. 168–176, 2017. [Online]. Available: <http://dx.doi.org/10.1016/j>

- [19] Y. Tang, Z. Zhang, R. Wang, Z. Hai, C. Xue, W. Zhang, and S. Yan, "Refractive index sensor based on fano resonances in metal-insulator-metal waveguides coupled with resonators," *Sensors*, vol. 17, no. 4, p. 784, 2017.
- [20] Zhao, Tonggang & Yu, Shilin. (2018). Ultra-High Sensitivity Nanosensor Based on Multiple Fano Resonance in the MIM Coupled Plasmonic Resonator. *Plasmonics*. 13. 1-6. 10.1007/s11468-017-0610-5.
- [21] Al Mahmud, R., Faruque, M.O. & Sagor, R.H. Plasmonic Refractive Index Sensor Based on Ring-Type Pentagonal Resonator with High Sensitivity. *Plasmonics* **16**, 873–880 (2021).
- [22] Xiao, G.; Xu, Y.; Yang, H.; Ou, Z.; Chen, J.; Li, H.; Liu, X.; Zeng, L.; Li, J. High Sensitivity Plasmonic Sensor Based on Fano Resonance with Inverted U-Shaped Resonator. *Sensors* **2021**, *21*, 1164.
- [23] Khani, Shiva & Hayati, Mohsen. (2021). An ultra-high sensitive plasmonic refractive index sensor using an elliptical resonator and MIM waveguide. *Superlattices and Microstructures*. 156. 106970. 10.1016/j.spmi.2021.106970.
- [24] Junxiong Chai, Yiyuan Xie, Liangyi Zhang, Yichen Ye, Bocheng Liu, Xiao Jiang, Rong Yang, Jing Tan, A novel plasmonic device: Filtering and switching functions with quasi-rectangular spectrum based on dual Fano resonances, *Optics & Laser Technology*, Volume 157, 2023, 108692, ISSN 0030-3992
- [25] Butt, M.A., Kazanskiy, N.L. & Khonina, S.N. Highly Sensitive Refractive Index Sensor Based on Plasmonic Bow Tie Configuration. *Photonic Sens* **10**, 223–232 (2020).
- [26] Z. Chen, L. Yu, L. Wang, G. Duan, Y. Zhao, and J. Xiao, "A refractive index nanosensor based on fano resonance in the plasmonic waveguide system," *IEEE Photonics Technology Letters*, vol. 27, no. 16, pp. 1695–1698, 2015.
- [27] F. Chen and D. Yao, "Realizing of plasmon fano resonance with a metal nanowall moving along mim waveguide," *Optics Communications*, vol. 369, pp. 72–78, 2016.
- [28] M. R. Rakhshani and M. A. Mansouri-Birjandi, "Utilizing the metallic nanorods in hexagonal configuration to enhance sensitivity of the plasmonic racetrack resonator in sensing application," *Plasmonics*, vol. 12, no. 4, pp. 999–1006, 2017.
- [29] E. Rafiee, R. Negahdari, and F. Emami, "PT SC," *Photonics and Nanostructures - Fundamentals and Applications*, 2018. [Online]. Available: <https://doi.org/10.1016/j.photonics.2018.11.006>

- [30] S. Ghorbani, M. A. Dashti, and M. Jabbari, "Plasmonic nano-sensor based on metal-dielectric-metal waveguide with the octagonal cavity ring," *Laser Physics*, vol. 28, no. 6, p. 066208, 2018.
- [31] Y. Zhang and M. Cui, "Refractive index sensor based on the symmetric mim waveguide structure," *Journal of Electronic Materials*, vol. 48, no. 2, pp. 1005–1010, 2019.
- [32] N. L. Kazanskiy and M. A. Butt, "Enhancing the sensitivity of a standard plasmonic MIM square ring resonator by incorporating nanodots in the cavity," vol. 12, no. 1, pp. 1–3, 2020.
- [33] M. A. Butt, S. N. Khonina, and N. L. Kazanskiy, "Plasmonic refractive index sensor based on M-I-M square ring resonator," *2018 International Conference on Computing, Electronic and Electrical Engineering, ICE Cube 2018*, pp. 1–4, 2019.
- [34] Z. Zhang, J. Yang, X. He, J. Zhang, J. Huang, D. Chen, and Y. Han, "Plasmonic refractive index sensor with high figure of merit based on concentric-rings resonator," *Sensors*, vol. 18, no. 1, p. 116, 2018.
- [35] D. G. Rabus, *Integrated ring resonators*. Springer, 2007.
- [36] M. Butt, S. Khonina, and N. Kazanskiy, "Plasmonic refractive index sensor based on mim square ring resonator," in *2018 International Conference on Computing, Electronic and Electrical Engineering (ICE Cube)*. IEEE, 2018, pp. 1–4.
- [37] K. Ahmed, F. Ahmed, S. Roy, B. K. Paul, M. N. Aktar, D. Vigneswaran, and M. S. Islam, "Refractive index-based blood components sensing in terahertz spectrum," *IEEE Sensors Journal*, vol. 19, no. 9, pp. 3368–3375, 2019.
- [38] Mahmud, R.A., Faruque, Md.O. and Sagor, R.H. 2021. Plasmonic Refractive Index Sensor Based on Ring-Type Pentagonal Resonator with High Sensitivity - *Plasmonics*. Available at: <https://link.springer.com/article/10.1007/s11468-020-01357-7>.
- [39] Rabiul Al Mahmud, Md. Omar Faruque, Rakibul Hasan Sagor, A highly sensitive plasmonic refractive index sensor based on triangular resonator, *Optics Communications*, Volume 483, 2021, 126634, ISSN 0030-4018, <https://doi.org/10.1016/j.optcom.2020.126634>. (<https://www.sciencedirect.com/science/article/pii/S003040182031052X>)